Biomedical Engineering: Applications, Basis and Communications, Vol. 23, No. 3 (2011) 237–244
DOI: 10.4015/S1016237211002578

OPTIMAL CONCENTRATIONS OF GADOVIST IN T_1-WEIGHTED MAGNETIC RESONANCE IMAGING: PHANTOM STUDY AND COMPUTER SIMULATION

Chia-Chi Hsiao*, Po-Chou Chen†, Huay-Ben Pan*
and Jo-Chi Jao‡,§

*Department of Radiology, Kaohsiung Veterans General Hospital
Kaohsiung 813, Taiwan

†Department of Biomedical Engineering, I-SHOU University
Kaohsiung 824, Taiwan

‡Department of Medical Imaging and Radiological Sciences
Kaohsiung Medical University, Kaohsiung 807, Taiwan
§jochja@kmu.edu.tw

Accepted 20 April 2011

ABSTRACT

Contrast-Enhanced Magnetic Resonance Imaging (CE-MRI) has been widely used in the diagnosis of lesions. Many contrast agents with various chemical and pharmacokinetic properties have been developed for clinical use. The signal-to-noise ratio (SNR) and contrast-to-noise ratio (CNR) after the contrast agent administration depend on many factors, e.g. category and injected dosage of contrast agents, field strength of magnetic resonance (MR) scanner, slew rate of gradient, type of radiofrequency coil, reconstruction algorithm, pulse sequences, and so on. Gadovist is a newly developed contrast agent with high formulation of 1.0 M. It has been used in MR angiography and perfusion studies. The aim of this study is to investigate the optimal concentrations of Gadovist in MR T_1-weighted (T1W) images from phantom study and computer simulation. A phantom made of 21 test tubes with various concentrations of Gadovist (0–160 mM) was investigated. All the studies were performed on a 1.5-T clinical whole-body scanner. Four T1W pulse sequences, including two-dimensional spoiled gradient echo (2DSPGR), three-dimensional fast spoiled gradient echo (3DFSPGR), conventional spin echo (CSE), and inversion recovery (IR) were employed to produce T1W images. The CNR values were calculated from regions of interest (ROIs) of all test tubes and the optimal concentration for each pulse sequence was determined. The T_1 and T_2 values of the phantom were also measured to obtain the relaxivities (r_1 and r_2). Afterward, the optimal concentration for each pulse sequence could be obtained from computer simulation by using the r_1 and r_2 values. The results showed that the measured optimal concentrations for 2DSPGR, 3DFSPGR, CSE and IR are 10, 20, 2.5, and 2.5 mM, respectively. The r_1 and r_2 values of the Gadovist phantom are 4.1 and 5.7 $mM^{-1}s^{-1}$, respectively. The optimal concentrations obtained from computer simulation are 13.5, 22.8, 2.0, and 2.7 mM for 2DSPGR, 3DFSPGR, CSE, and IR, respectively. The optimal concentrations obtained from computer simulation and phantom study are in good agreement.

Keywords: Gadovist; Spin echo; Spoiled gradient echo; Inversion recovery; Pulse sequence.

§Corresponding author: Jo-Chi Jao, Department of Medical Imaging and Radiological Sciences, Kaohsiung Medical University, Kaohsiung 807, Taiwan. Tel: +886-7-3121101 ext. 2356-14; Fax: +886-7-3113449; E-mail: jochja@kmu.edu.tw

INTRODUCTION

Magnetic resonance imaging (MRI) has been developing rapidly and is a very important modality used in clinics for lesion detection and treatment follow-up.[1–10] MRI can demonstrate high contrast between soft tissues. In addition, it is noninvasive and produces no ionizing radiation. Because of the administration of contrast agents, the contrast of MRI improves significantly. Contrast-enhanced MRI (CE-MRI) has been widely used in angiography and perfusion.[11–20] Gd-DTPA (Magnevist, Schering AG, Berlin, Germany) is the first contrast agent approved by US Food and Drug Administration (FDA) in 1988. It is a nonspecific extracellular contrast agent. Nowadays, Gd-DTPA is the most commonly used contrast agent in the world.[21–25] Novel contrast agents have emerged for different purposes since 1988. Gadovist (Gadobutrol, Schering AG, Berlin, Germany) is a contrast agent, which has recently become clinically available. It is a neutral, hydrophilic, and macrocyclic contrast agent. Because of its low osmolality and viscosity in comparison to Gd-DTPA, it has been supplied at 1.0-M formulation, which is higher than that of Gd-DTPA (0.5 M). Consequently, Gadovist can be injected with smaller volume. It is also an extracellular contrast agent and excreted from kidneys readily.[26–30]

Both Gd-DTPA and Gadovist are paramagnetic contrast agents that can shorten both longitudinal (T_1) and transverse (T_2) relaxation times. The signal-to-noise ratio (SNR) and contrast-to-noise ratio (CNR) will be changed as well. The reduction of both relaxation times depends on the concentrations of the contrast agents. The relationship between the relaxation times and the concentration of a contrast agent is shown as follows[31]:

$$1/T_1 = 1/T_{10} + r_1[c] \quad (1a)$$

$$1/T_2 = 1/T_{20} + r_2[c], \quad (1b)$$

where r_1 is defined as the longitudinal relaxivity, r_2 is the transverse relaxivity, T_1 is the longitudinal relaxation time, T_2 is the transverse relaxation time of a phantom or tissue with concentration [c] of the contrast agent, T_{10} is the longitudinal relaxation time, and T_{20} is the transverse relaxation time of a phantom or tissue in absence of any contrast agent.

Equation (1) shows the higher the concentration of the contrast agent, the shorter the relaxation time of protons. The SNR and CNR values depend not only on T_1 and T_2 values of a phantom or tissue but also on the choice of a pulse sequence and scanning parameters. Stalder measured the optimal concentration of Gadovist using a fast low angle shot (FLASH) pulse sequence.[32] In our previous studies, the optimal concentrations of Gd-DTPA and Gd-DTPA-BMA in several T1W images were measured.[33] In this study, a phantom made of Gadovist with various concentrations was investigated by using four T1W pulse sequences, including two-dimensional spoiled gradient echo (2DSPGR), three-dimensional fast spoiled gradient echo (3DFSPGR), conventional spin echo (CSE) and inversion recovery (IR). The 2D and 3D SPGR pulse sequences have been widely used in MR angiography and CE-MRI.[12,14,21,23] Although CSE and IR take longer scanning time, because they possess less susceptibility sensitivity, they still can be used in some area, for example, the detection of multiple sclerosis and brain metastasis, etc.[9,13,20] Different scanning parameters and pulse sequences will result in different optimized concentrations. The optimal concentrations were defined to achieve the maximum CNR for each pulse sequence and were first obtained from the phantom measurements. Then, the T_1 and T_2 values of the phantom with various concentrations of Gadovist were evaluated to obtain the relaxivity values (r_1 and r_2). Finally, the optimal concentrations were obtained from computer simulation and were compared with those values obtained from the phantom study mentioned above.

MATERIALS AND METHODS

All the MRI studies were performed on a whole-body 1.5-T MR scanner (GE Signa HDxt, GE Medical Systems, Milwaukee, WI, USA) with a quadrature head coil.

Optimal Concentration Measurements

Twenty one 15-ml test tubes containing 10 ml distilled water doped with different concentrations (0, 0.1, 0.2, 0.4, 0.8, 1.25, 2.5, 5, 10, 15, 20, 25, 30, 35, 40, 60, 80, 100, 120, 140, 160 mM) of Gadovist were prepared. These test tubes were fixed in a polystyrene holder and then placed inside the head coil. After the three-plane localizer scan, the phantom was scanned by a series of pulse sequences. Four pulse sequences, including 2DSPGR, 3DFSPGR, CSE, and IR, were used for scanning. The parameters of these pulse sequences used in this study are listed in Table 1.

All the MR images were transferred to an Advantage Window workstation for regions of interest (ROIs) measurements. Once the ROI values of these 21 test tubes and one background outside the phantom were obtained, the SNR and CNR values of the test tubes

Table 1. Parameters of Various Pulse Sequences Used for Optimal Concentration Measurements.

Pulse Sequences	FA (°)	TR/TE/TI (ms)	Matrix	BW (kHz)	THK (mm)	NEX	FOV (cm^2)
2DSPGR	50	13/4.5/null	256 × 160	31	5	4	24 × 24
3DFSPGR	35	6.1/1.9/null	256 × 224	31.3	1.4	1	24 × 24
CSE	90	350/14/null	256 × 192	15.6	5.0	1	24 × 24
IR	180–90	400/30/200	256 × 160	31.3	5	1	24 × 24

with various Gadovist concentrations were calculated by Eqs. (2) and (3), respectively.

$$SNR(c) = S(c)/\sigma_{BGD} \tag{2}$$

$$CNR(c) = SNR(c) - SNR(0), \tag{3}$$

where $S(c)$ is the MR signal intensity of a test tube with the concentration [c] of Gadovist, $SNR(0)$ is the SNR of distilled water only and σ_{BGD} is the standard deviation of the background signal. The optimal concentration was determined by the maximum value of CNR.

T_1 and T_2 Measurements

The same phantom as mentioned above was used for T_1 and T_2 measurement. The parameters for T_1 measurement were listed as follows: field of view (FOV) = 24 × 24 cm^2, matrix size = 256 × 192, slice thickness = 5 mm, Bandwidth (BW) = 15.6 kHz, number of excitation (NEX) = 1, TE = 14 ms and TR = 200–3000 ms with 200 ms increments. The parameters for T_2 measurement were the same as the T_1 measurement except TR = 3000 ms and TE = 15, 30, 45, 60, 75, 90, 120, 150, 200, 300, 400, 600, 800, 1000, 1200, 1400, 1600, 1800 ms. After three-plane localizer scan, one coronal image was obtained for each TE/TR. All the MR images were transferred to an Advantage Window workstation for ROI measurements. Once the ROI values of these 21 test tubes were obtained, the T_1 and T_2 values for each tube with various Gadovist concentrations were obtained by nonlinear least square fitting according to Eqs. (4) and (5), respectively.[34]

$$S = M\{1 - 2\exp[-(TR - 0.5\,TE)/T_1] + \exp(-TR/T_1)\} \tag{4}$$

$$S = M\exp(-TE/T_2), \tag{5}$$

where S is the MR signal intensity, M is proportional to the net magnetization, TR is the repetition time, TE is the echo time, T_1 is the longitudinal relaxation time, and T_2 is the transverse relaxation time.

Once the $1/T_1$ and $1/T_2$ values were obtained, the r_1 and r_2 values could be determined by linear regression according to Eq. (1). A commercial software (Sigmaplot, version 9.01, Systat Software, CA, USA) was used for nonlinear least square fitting and linear regression.

Computer Simulation

Once the T_{10}, T_{20}, r_1, and r_2 values were obtained, the T_1 and T_2 values for certain concentration could be obtained from Eq. (1). Then, the MR signal intensities for 2DSPGR and 3DFSPGR were calculated according to Eq. (6) and those for CSE and IR were calculated according to Eqs. (7) and (8), respectively.[34]

$$S = M\frac{\sin(FA)(1 - \exp(-TR/T_1))}{1 - \cos(FA)\exp(-TR/T_1)} \times \exp(-TE/T_2^*) \tag{6}$$

$$S = M\{1 - 2\exp[-(TR - 0.5\,TE)/T_1] + \exp(-TR/T_1)\}\exp(-TE/T_2) \tag{7}$$

$$S = M\{1 - 2\exp(-TI/T_1) + \exp(-TR/T_1)\} \times \exp(-TE/T_2), \tag{8}$$

where S is the MR signal intensity, M is proportional to the net magnetization, FA is the flip angle, TR is the repetition time, TE is the echo time, TI is the inversion time, T_1 is the longitudinal relaxation time, and T_2 is the transverse relaxation time.

First, the assumption of $T_2 = T_2^*$ was made in computer simulation. The simulated MR signal intensity corresponding to the optimal concentration of phantom measurements was set to be equal to the peak signal intensity of the phantom for the determination of M value. The noise levels used in computer simulation were set to be equal to that of phantom as well. Then, the SNR and CNR values for these four pulse sequences were calculated according to Eqs. (2) and (3). Finally, the simulated optimal concentrations were determined from the maximum CNR values.

RESULTS

Optimal Concentration Measurements

One representative 3DFSPGR image is shown in Fig. 1(A). The concentration of Gadovist varied from 0 to 160 mM. The MR signal versus concentration curve is

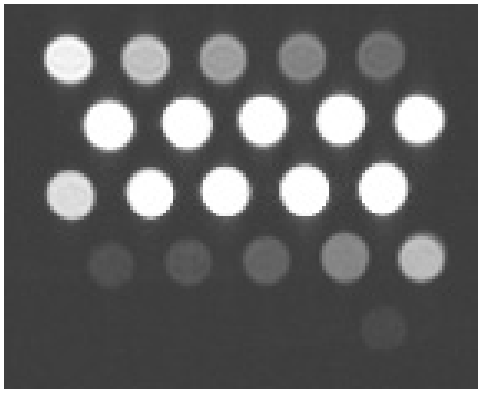

(A)

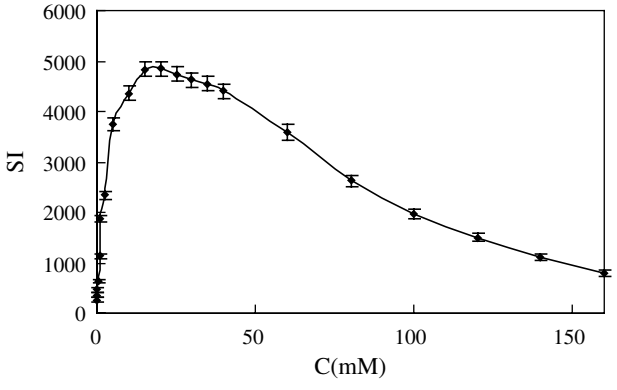

(B)

Fig. 1 **(A)** One coronal MR image of the Gadovist phantom using 3DFSPGR pulse sequence, **(B)** Signal–concentration curve of the Gadovist phantom (concentrations of Gadovist from top to bottom and from left to right. Row 1: 80, 100, 120, 140, 160; Row 2: 25, 30, 35, 40, 60; Row 3: 2.5, 5, 10, 15, 20; Row 4: 0.1, 0.2, 0.4, 0.8, 1.25; Row 5: 0 mM).

shown in Fig. 1(B). It demonstrates that the MR signal intensity increases with the concentration of Gadovist to the maximum value first, and then decreases with the concentration of Gadovist. The CNR versus concentration curves for these four pulse sequences are shown in Fig. 2. The CNR value increases first, reaches the maximum value, and then decreases as the concentration of Gadovist increases. Table 2 shows the measured

Table 2. Optimal Concentrations Related to the Maximum CNR Values for Various Pulse Sequences.

Pulse Sequence	$C_{\text{opt-}m}$ (mM)[a]	$C_{\text{opt-}s}$ (mM)[b]
2DSPGR	10	13.5
3DFSPGR	20	22.8
CSE	2.5	2.0
IR	2.5	2.7

[a]Phantom measurement.
[b]Computer simulation.

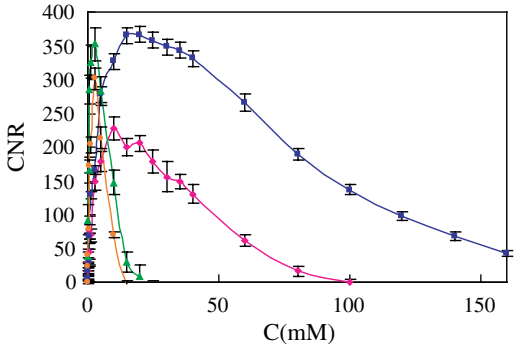

(A)

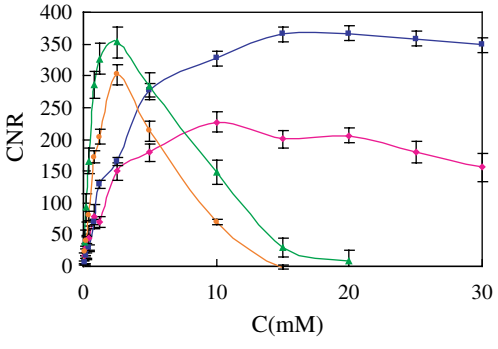

(B)

Fig. 2 **(A)** CNR–concentration curve of the Gadovist phantom for 2DSPGR (♦), 3DFSPGR (■), CSE (▲), and IR (•) pulse sequences. **(B)** The spread of the low concentration region of **(A)**.

optimal concentrations ($C_{\text{opt}-m}$) corresponding to the maximum CNR for each pulse sequence.

T_1 and T_2 Measurement

The T_1 and T_2 fitting curves for 0.2 and 1.25 mM Gadovist obtained from Eqs. (4) and (5) are shown in Fig. 3. The T_1 values for 0.2 and 1.25 mM Gadovist are 882.1 and 187.6 ms, respectively. The T_1 value of 0.2 mM Gadovist is higher than that of 1.25 mM Gadovist, therefore, the MR signal intensity increases with TR is slower than that of 1.25 mM Gadovist. The MR signal intensity of 1.25 mM Gadovist increases rapidly and reaches the plateau in a very short interval. The fitting results are good; $R^2 = 0.9996$ and $R^2 = 0.9899$ for 0.2 and 1.25 mM Gadovist, respectively. The T_1 value becomes smaller when the concentration of Gadovist increases. The T_1 value is too small to be measured when the concentration of Gadovist is higher than 5.0 mM. From the linear regression (0–5 mM), r_1 value is 4.1 s^{-1} mM^{-1} ($R^2 = 0.9883$). The T_2 values for 0.2 and 1.25 mM Gadovist are 591.80 and 170.30 ms, respectively. The T_2 value of 1.25 mM Gadovist is lower than that of 0.2 mM Gadovist. In summary, the MR

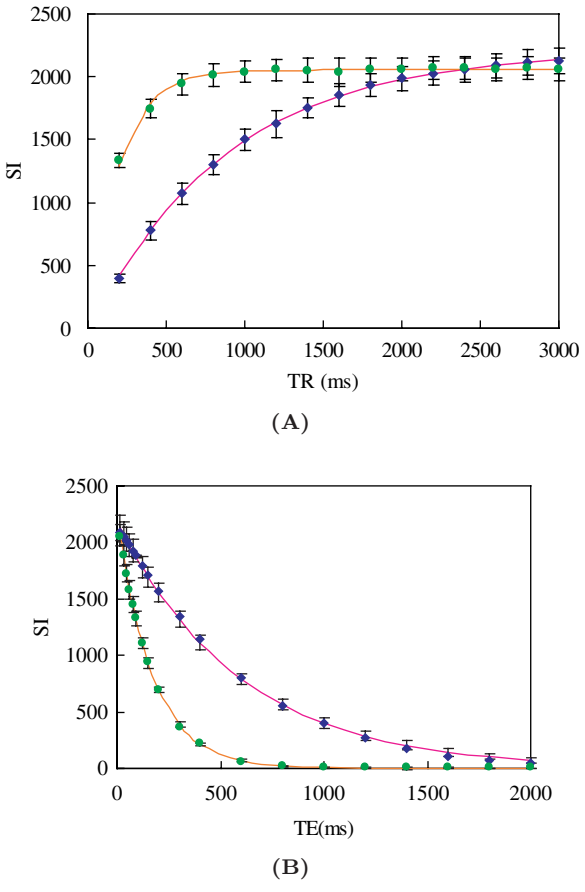

Fig. 3 **(A)** T_1 and **(B)** T_2 fitting curves for 0.2 (♦) and 1.25 mM (•) Gadovist.

signal decay of 1.25 mM Gadovist with TE is faster than that of 0.2 mM Gadovist. The fitting results are good for both 0.2 mM ($R^2 = 0.9992$) and 1.25 mM ($R^2 = 0.9999$) Gadovist, respectively. The fitting results of T_2 values become worse when the concentration of Gadovist is higher than 30 mM. According to the linear regression (0–5 mM), r_2 value is 5.70 $s^{-1}mM^{-1}$ ($R^2 = 0.9952$). The $1/T_1$ and $1/T_2$ values versus concentration curves are shown in Fig. 4.

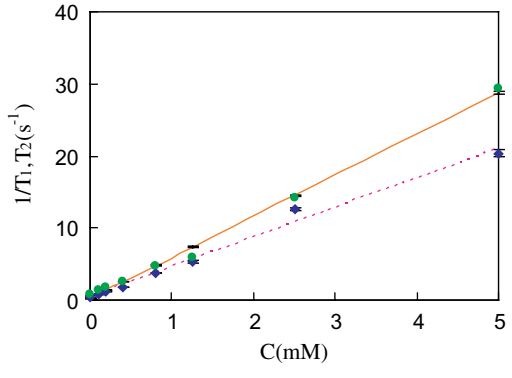

Fig. 4 The linear regression of $1/T_1$ (♦) and $1/T_2$ (•) with concentrations of Gadovist.

Computer Simulation

The CNR–concentration curves from the computer simulation for various pulse sequences are shown in Fig. 5. The CNR value increases first to the peak value and then decreases. The optimal concentrations from the computer simulation ($C_{\text{opt-}s}$) are also listed in Table 2.

DISCUSSION

The MR signal intensity is a function of T_1 and T_2 values. According to Eq. (1), both T_1 and T_2 values decrease as the concentration of paramagnetic contrast agents increases. Therefore, the intensity of MR signal increases or decreases with concentrations depending on the predomination of T_1 or T_2 effect.[31] The CNR values change with the concentration of contrast agents, which have same tendency in both phantom measurements and computer simulations. The CNR values initially increase to the peak values as the concentration of the contrast agent increases because the T_1 effect is greater than the T_2 effect. Afterward, they begin to decrease as the concentration of contrast agent increases because the T_2 effect becomes greater than the T_1 effect. When the signal intensity of a certain test tube is less than that of the distilled water, the CNR becomes negative. The range of negative CNR values implies that the heavy T_2 effect occurs when the contrast agent's concentration is high enough. Apparently, one should avoid such situation in which the concentration of the contrast agent exceeds the optimal concentration in the use of T1W images.

Both the CNR–concentration curves from computer simulations and phantom measurements have the same tendency, i.e. the CNR values increase with concentrations to the peak values and then decrease afterward. The CNR values from both methods match well when the concentrations of Gadovist are low. The deviation between the CNR values obtained from these two methods becomes larger when the concentration of Gadovist increases. Here, we determined the M values in Eqs. (6)–(8) by normalizing the signal intensity to the peak values obtained from phantom measurements. The T_{10}, T_{20}, relaxivity values (r_1, r_2) and noise levels were also obtained from the phantom measurements. The relaxivity values are well known to be dependent on field strength, temperature and solvents, etc. Herein, relaxivity values were measured in room temperature with distilled water as a solvent. Consequently, it might be different from those values measured in 37°C and with plasma as a solvent.[35,36] The relaxivity values in this study were obtained by linear regression from 0–5 mM. For simplicity, we assumed that there existed

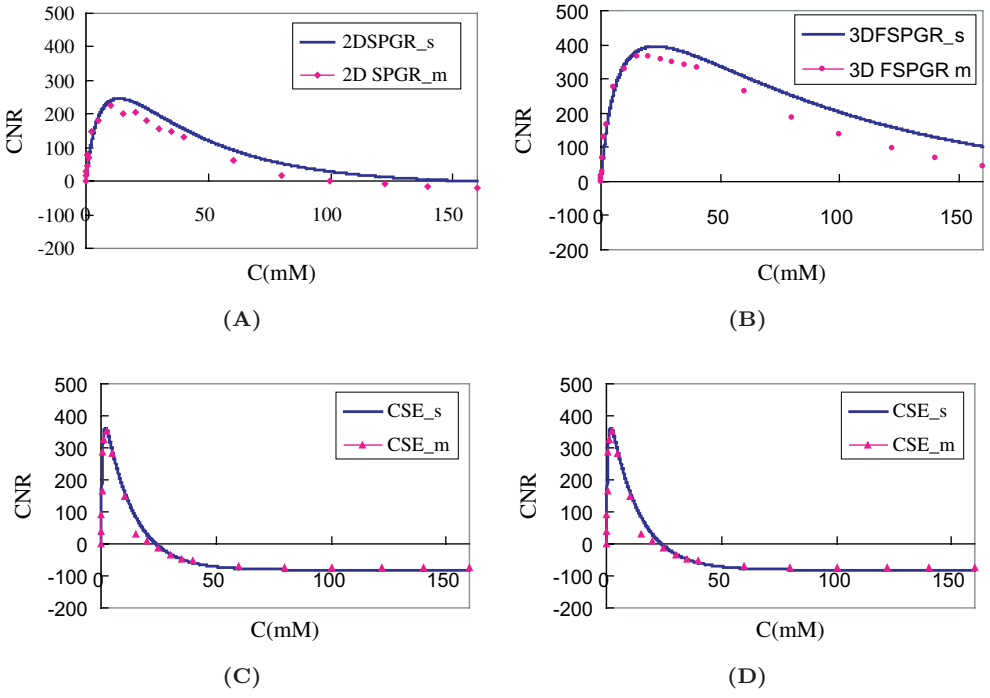

Fig. 5 The CNR–concentration curves of **(A)** 2DSPGR, **(B)** 3DFSPGR, **(C)** CSE, and **(D)** IR pulse sequences from computer simulations (_s) and phantom measurements (_m).

only one r_1 or r_2 relaxivity value for all concentrations of Gadovist, and extended the linearity from 0 to 160 mM during computer simulation. It appeared that the relaxivity value could be different for Gadovist at high concentration and that might need to be further verified. On the other hand, it probably was one of the reasons that caused the mismatch of the CNR concentration curves between the computer simulations and phantom measurements. Furthermore, the assumption of $T_2 = T_2^*$ might not be applicable for cases of high concentration of Gadovist. Incidentally, the r_2 value of $5.7\,\mathrm{mM^{-1}s^{-1}}$ obtained in this study was quite similar to Stalder's result ($r_2 = 5.5\,\mathrm{mM^{-1}s^{-1}}$). Spin-echo pulse sequence was used in both studies. In general, T_1 values were measured by using saturation spin echo or inversion recovery pulse sequence.[32,37,38] Here, the r_1 value of 4.1 $\mathrm{mM^{-1}s^{-1}}$ obtained by using a spin-echo pulse sequence was also similar to Stalder's result ($r_1 = 4.7\,\mathrm{mM^{-1}s^{-1}}$) obtained by using a inversion recovery pulse sequence with distilled water as a solvent at room temperature. Even though there existed some discrepancy as discussed above while applying computer simulations, the results showed that the optimal concentrations obtained from both phantom measurements and computer simulations were in good agreement. The optimal concentrations might be different for the same pulse sequence but with different scan parameters, i.e. TR, TE and FA etc. Even so, one could still use the measured r_1, r_2, T_{10} and T_{20} values to derive CNR values and obtain simulated optimal concentrations with various parameters from computer simulations.

CONCLUSIONS

Nowadays, there are several contrast agents available in clinic for CE-MRI.[39–43] Gadovist is the first commercial contrast agent with high formulation of 1.0 M. In this study, the optimal concentrations of Gadovist for 2DSPGR, 3DFSPGR, CSE, and IR T1W pulse sequences were evaluated. The results show that both the phantom measurements and computer simulations are in good agreement. It might be helpful for diagnosis and treatment follow-up by the appropriate use of contrast agents in clinic. It implies that the concentrations higher than the optimal concentrations should be avoided. However, to correlate the optimal concentration with respect to the optimal injecting dose in routine examinations requires further investigations.

ACKNOWLEDGMENT

The authors would like to thank Kaohsiung Veteran General Hospital in Taiwan, the Republic of China, for financial support by the grant VGSKS98-066 and National Science Council in Taiwan under the grant No. NSC99-2221-E-214-008.

REFERENCES

1. Liu Q, Chen J, Li H *et al.*, Hepatocellular carcinoma with bile duct tumor thrombi: Correlation of magnetic resonance imaging features to histopathologic manifestations, *Eur J Radiol* **76**:103–109, 2010.
2. Khan AS, Hussain HK, Johnson TD *et al.*, Value of delayed hypointensity and delayed enhancing rim in magnetic resonance imaging diagnosis of small hepatocellular carcinoma in the cirrhotic liver, *J Magn Reson Imaging* **32**:360–366, 2010.
3. Jacobs MA, Stearns V, Wolff AC *et al.*, Multiparametric magnetic resonance imaging, spectroscopy and multinuclear (^{23}Na) imaging monitoring of preoperative chemotherapy for locally advanced breast cancer, *Acad Radiol* **17**:1477–1485, 2010
4. Graubard BI, Freedman AN, Gail MH, Five-year and lifetime risk of breast cancer among US subpopulations: Implications for magnetic resonance imaging screening, *Cancer Epidemiol Biomarkers Prev* **19**:2430–2436, 2010.
5. Jeong IG, Kim JK, Cho KS *et al.*, Diffusion-weighted magnetic resonance imaging in patients with unilateral prostate cancer on extended prostate biopsy: Predictive accuracy of laterality and implications for hemi-ablative therapy, *J Urol* **184**:1963–1969, 2010.
6. Sciarra A, Panebianco V, Ciccariello M *et al.*, Magnetic resonance spectroscopic imaging (1H-MRSI) and dynamic contrast-enhanced magnetic resonance (DCE-MRI): Pattern changes from inflammation to prostate cancer, *Cancer Invest* **28**:424–432, 2010.
7. Wang JZ, Mayr NA, Zhang D *et al.*, Sequential magnetic resonance imaging of cervical cancer: The predictive value of absolute tumor volume and regression ratio measured before, during, and after radiation therapy, *Cancer* **116**:5093–5101, 2010.
8. Chung HH, Kang KW, Cho JY *et al.*, Role of magnetic resonance imaging and positron emission tomography/computed tomography in preoperative lymph node detection of uterine cervical cancer, *Am J Obstet Gynecol* **203**:156.e1–5, 2010.
9. Yamamoto S, Takano H, Motoori K *et al.*, Detection of nasopharyngeal carcinoma: Fast short time inversion recovery images compared with fat suppression, contrast enhanced T1 weighted spin echo images, *British J Radiol* **74**:805–810, 2001.
10. Guimaraes AR, Tabatabei S, Dahl D *et al.*, Pilot study evaluating use of lymphotrophic nanoparticle-enhanced magnetic resonance imaging for assessing lymph nodes in renal cell cancer, *Urology* **71**:708–712, 2008.
11. Wieners G, Meyer F, Halloul Z *et al.*, Detection of Type II endoleak after endovascular aortic repair: Comparison between magnetic resonance angiography and blood-pool contrast agent and dual-phase computed tomography angiography, *Cardiovasc Intervent Radiol* **33**:1135–1142, 2010.
12. Wang CC, Liang HL, Hsiao CC *et al.*., Single-dose time-resolved contrast enhanced hybrid MR angiography in diagnosis of peripheral arterial disease: Compared with digital subtraction angiography, *J Magn Reson Imaging* **32**:935–942, 2010.
13. Kakeda S, Korogi Y, Hiai Y *et al.*, Detection of brain metastasis at 3T: Comparison among SE, IR-FSE and 3D-GRE sequences, *Eur Radiol* **17**:2345–2351, 2007.
14. Anzalone N, Scomazzoni F, Cirillo M *et al.*, Follow-up of coiled cerebral aneurysms: Comparison of three-dimensional time-of-flight magnetic resonance angiography at 3 tesla with three-dimensional time-of-flight magnetic resonance angiography and contrast-enhanced magnetic resonance angiography at 1.5 Tesla, *Invest Radiol* **43**:559–567, 2008.
15. Blml S, Schad LR, Scharf J *et al.*, A comparison of magnetization prepared 3D gradient-echo (MP-RAGE) sequences for imaging of intracranial lesions, *Magn Reson Imaging* **14**:329–335, 1996.
16. Kumar VA, Knopp EA, Zagzag D, Magnetic resonance dynamic susceptibility-weighted contrast-enhanced perfusion imaging in the diagnosis of posterior fossa hemangioblastomas and pilocytic astrocytomas: Initial results, *J Comput Assist Tomogr* **34**:825–829, 2010.
17. Liao W, Liu Y, Wang X *et al.*, Differentiation of primary central nervous system lymphoma and high-grade glioma with dynamic susceptibility contrast-enhanced perfusion magnetic resonance imaging, *Acta Radiol* **50**:217–225, 2009.
18. Jang YM, Oh YM, Seo JB *et al.*, Quantitatively assessed dynamic contrast-enhanced magnetic resonance imaging in patients with chronic obstructive pulmonary disease: Correlation of perfusion parameters with pulmonary function test and quantitative computed tomography, *Invest Radiol* **43**:403–410, 2008.
19. Inglese M, Park SJ, Johnson G *et al.*, Deep gray matter perfusion in multiple sclerosis: Dynamic susceptibility contrast perfusion magnetic resonance imaging at 3 T, *Arch Neurol* **64**:196–202, 2007.
20. Evans AL, Widjaja E, Connolly DJ *et al.*, Cerebral perfusion abnormalities in children with Sturge-Weber syndrome shown by dynamic contrast bolus magnetic resonance perfusion imaging, *Pediatrics* **117**:2119–2125, 2006.
21. Muthupillai R, Douglas E, Huber S *et al.*, Direct comparison of sensitivity encoding (SENSE) accelerated and conventional 3D contrast enhanced magnetic resonance angiography (CE-MRA) of renal arteries: Effect of increasing spatial resolution, *J Magn Reson Imaging* **31**:149–159, 2010.
22. Spencer RG, Fishbein KW, Cheng A *et al.*, Compatibility of Gd-DTPA perfusion and histologic studies of the brain, *Magn Reson Imaging* **24**:27–31, 2006.
23. Lyng H, Vorren AO, Sundfør K *et al.*, Assessment of tumor oxygenation in human cervical carcinoma by use of dynamic Gd-DTPA-enhanced MR imaging, *J Magn Reson Imaging* **14**:750–756, 2001.
24. Sabir N, Sungurtekin U, Erdem E *et al.*, Gentic resonance imaging with rectal Gd-DTPA: New tool for the diagnosis of perianal fistula, *Int J Colorectal Dis* **15**:317–322, 2000
25. Stapa RZ, Jakubowski W, Dabrowska E *et al.*, Magnetic resonance imaging differentiation of adrenal masses at 1.5 T: T2-weighted images, chemical shift imaging, and Gd-DTPA dynamic studies, *MAGMA* **4**:163–179, 1996.

26. Kim ES, Chang JH, Choi HS *et al.*, Dagnostic yield of double-dose gadobutrol in the detection of brain metastasis: Intraindividual comparison with double-dose gadopentetate dimeglumine, *Am J Neuroradiol* **31**:1055–1058, 2010.
27. Kramer H, Runge VM, Naul LG *et al.*, Brain MRI with single-dose (0.1 mmol/kg) Gadobutrol at 1.5 T and 3 T: Comparison with 0.15 mmol/kg Gadoterate meglumine, *Am J Roentgenol* **194**:1337–1342, 2010.
28. Forsting M, Palkowitsch P, Prevalence of acute adverse reactions to gadobutrol — A highly concentrated macrocyclic gadolinium chelate: Review of 14,299 patients from observational trials, *Eur J Radiol* **74**:e186–e192, 2010.
29. Achenbach M, Figiel JH, Burbelko M *et al.*, Prospective comparison of image quality and diagnostic accuracy of 0.5 molar gadobenate dimeglumine and 1.0 molar gadobutrol in contrast-enhanced run-off magnetic resonance angiography of the lower extremities, *J Magn Reson Imaging* **5**:1166–1171, 2010.
30. Attenberger UI, Runge VM, Morelli JN *et al.*, Evaluation of gadobutrol, a macrocyclic, nonionic gadolinium chelate in a brain glioma model: Comparison with gadoterate meglumine and gadopentetate dimeglumine at 1.5 T, combined with an assessment of field strength dependence, specifically 1.5 versus 3 T, *J Magn Reson Imaging* **1**:549–555, 2010.
31. Woodward P, Freimarck R, *MRI for Technologists*, pp. 146 (McGraw-Hill Inc., New York, USA), 1995.
32. Stalder AF, Elverfeldt DV, Paul D *et al.*, Variable echo time imaging: Signal characteristics of 1-m gadobutrol Contrast Agent at 1.5 and 3T, *Magn Reson Med* **59**:113–123, 2008.
33. Hsiao CC, Jao JC, Ting YN *et al.*, Optimal Dose of MR Contrast Agent in T1-weighted MRI, *Biomed Eng Appl Basic Comm* **16**:331–336, 2004.
34. Liang ZP, Lauterbur PC, *Principles of Magnetic Resonance Imaging: A signal Processing Perspective*, pp. 223–227 (Institute of Electrical and Electronics Engineers, Inc., New York, USA), 2000.
35. Pintaske J, Martirosian P, Graf H *et al.*, Relaxivity of gadopentetate dimeglumine (magnevist), gadobutrol (gadovist), and gadobenate dimeglumine (MultiHance) in human blood plasma at 0.2, 1.5, and 3 Tesla, *Invest Radiol* **41**:213–221, 2006.
36. Sasaki M, Shibata E, Kanbara Y *et al.*, Enhancement effects and relaxivities of gadolinium-DTPA at 1.5 versus 3 Tesla: A phantom study, *Magn Reson Med Sci* **4**:145–149, 2005.
37. Simon GH, Bauer J, Saborovski O *et al.*, T1 and T2 relaxivity of intracellular and extracellular USPIO at 1.5 T and 3 T clinical MR scanning, *Eur Radiol* **16**:738–745, 2006.
38. Jao JC, Chen PC, Ting YN *et al.*, The impact of factor TE on the measurement of T1 relaxivity, *Biomed Eng Appl Basic Comm* **20**:277–285, 2008
39. Moriarty JM, Finn JP, Fonseca CG, Contrast agents used in cardiovascular magnetic resonance imaging: Current issues and future directions, *Am J Cardiovasc Drugs* **10**:227–237, 2010.
40. Geraldes CF, Laurent S, Classification and basic properties of contrast agents for magnetic resonance imaging, *Contrast Media Mol Imaging* **4**:1–23, 2009.
41. Frenzel T, Lengsfeld P, Schirmer H *et al.*, Stability of gadolinium-based magnetic resonance imaging contrast agents in human serum at 37°C, *Invest Radiol* **43**:817–828, 2008.
42. Zhang Z, Nair SA, McMurry TJ, Gadolinium meets medicinal chemistry: MRI contrast agent development, *Curr Med Chem* **12**:751–778, 2005.
43. Lorusso V, Pascolo L, Fernetti C *et al.*, Magnetic resonance contrast agents, *Curr Pharm Des* **11**:4079–4098, 2005.